Proceedings of the ASME 2010 3rd Joint US-European Fluids Engineering Summer Meeting and 8th International Conference on Nanochannels, Microchannels, and Minichannels
FEDSM-ICNMM2010
August 1-5, 2010, Montreal, Canada

FEDSM-ICNMM2010-30893

LARGE EDDY SIMULATIONS OF JET FLOW INTERACTION WITHIN STAGGERED ROD BUNDLES

Nathaniel Salpeter
Texas A&M University
College Station, TX, USA
natesal@tamu.edu

Dr. Yassin Hassan
Texas A&M University
College Station, TX, USA

ABSTRACT

The present work investigates the turbulent jet flow mixing of downward impinging jets within a staggered rod bundle based on previous experimental work. Two inlet jets had Reynold's numbers of 11,160 and 6,250 and were chosen to coincide with available data [Amini and Hassan 2009]. Steady state simulations were initially carried out on a semi-structured polyhedral mesh of roughly 13.2 million cells following a sensitivity study over six different discretized meshes. Very large eddy simulations were carried out over the most refined mesh and continuous 1D wavelet transforms were used to analyze the dominant instabilities and how they propagate through the system in an effort to provide some insight into potential problems relating to structural vibrations due to turbulent instabilities. The presence of strong standing horseshoe vorticies near the base of each cylinder adjacent to an inlet jet was noted and is of potential importance in the abrasion wear of the graphite support columns of the VHTR if sufficient wear particles are present in the gas flow.

INTRODUCTION

The push for safer and more efficient nuclear reactors with less margin for risk has resulted in the need for high fidelity numerical simulations of reactor designs. In order to achieve the necessary confidence level in the simulations being conducted using current computational fluid dynamics (CFD) techniques, it is paramount that numerical models be validated against experimental data representative of phenomena likely to appear within a nuclear power plant.

The focus of this study is partly on the validation of numerical models against results previously published by Amini and Hassan [2009] but also on the identification of flow features seen in the numerical results for further investigation both experimentally and through CFD simulations. The experimental study was focused on jet impingement upon a lower plane within a bank of staggered rods parallel to the inlet jet axis, mimicking similar phenomena of the lower plenum of a very high temperature gas cooled reactor (VHTR). Two jets within the rod bundle were used with a single outlet to one side of the channel. This work details a numerical study aimed at making a contribution in the validation of numerical models for such nuclear applications by modeling the experimental facility within the Star-CCM+ v.3.06.006 CFD package and quantifying the level of agreement of the result with the experimental data. Additional analysis of the flow phenomenology seen in the CFD results was also performed. It is important to note that in the process of validating numerical models, the cases in which the models have discrepancies from the experimental results are just as important in the determination of model limits as are the results that match closely with the experimental data set.

In the case of mixing within the lower plenum mixing of the VHTR, the importance of such studies are to ensure the absence of hot streaking and hot spots as well as investigate possible locations of turbulence induced vibrations and abrasion within the support structure. Hot streaking is a phenomenon by which hot gas exits the reactor core and exhausts into the lower plenum but does not sufficiently mix prior to reaching the steam generator, thus causing hot spots within other plant components not specifically designed to handle such spikes in temperature.

One investigation at Sandia National Laboratory involves the numerical study of the effect of static helicoidal inserts inside the jet inlets in order to disrupt axial momentum and increase mixing [Rodriguez, El-Genk 2008]. This study looked at both jets with and without helicoidal inserts in the inlet jets; however, the focus of the work was on structures right in the wake of the jet as opposed to this study in which structures within the rod bundle will be investigated as well.

Studies have been done involving axial flow along rod arrays in which 'pulsing' phenomena are found between closely spaced rods. One experimental study investigates channel flows with varying sized rods within it [Rehme K. 1989]. Spectral analysis of the same channel conditions was done a few years later and found very regular azimuthal component fluctuations between the rods [Möller 1992]. The present study has high velocity jet impingement on a lower plane rather than

a uniform cross flow. The similarity with the pulsations of flow between the previous study and this work is in the regions between adjacent rods as well as between rods and adjacent walls. In these locations there is an updraft from the impinged jet striking the wall and moving upwards in the small space between the rods and the wall. In locations of flow past cylindrical rods, the generation of turbulent instabilities presents a structural concern with respect to vibration in the support rods of the VHTR.

Jet impingement studies using numerical methods have suggested the presence of different modes of flow structure in the impinged flow [Li et al. 2005]. In their study, numerical results indicated the presence of two modes downstream of the impingement location. One was that the flow remained along the lower plane and in the other the flow separated from the lower plane and flowed freely within the domain. In the case of the present study, flow within the rod bundle remained in the regime where the flow remained in contact with the impingement plane until coming in contact with the adjacent rods.

The necking of the jet and formation of ring vorticies has been observed in experimental works for round jets in the same range of Reynolds numbers as the present work [F. Shu *et al.* 2005]. In the case of a jet that has a top-hat profile as opposed to a Gaussian profile, a reduced distance (x/D) to the onset of vortex rings has been documented [New *et al* 2006]. Muzzammil and Gangadhariah [2003] experimentally investigated the presence of the primary horseshoe vortex formed around the base of a pier column in a crossflow and the key role that is played by this vortex in the scouring of the loose surrounding base material. Wear particles that are present in the gas flow after passing through the core may potentially act as an abrasive in locations with strong consistent vorticies over the lifespan of a reactor. Greenly and Iverson [1985] describe shadow zones as features observed in the wake of horseshoe vorticies just following an obstruction and before the onset of turbulent instabilities. This phenomenon of high inertia dust particles settling out of the bulk flow has been described by them as the reason for dust buildup just behind obstructions in windy conditions. When concerned with mixing levels, such dead zones should be kept in mind. The problem of suspended particles must be addressed in terms of the effect of particles in suspension as well as potential locations of coalescence. This study identifies potential locations of dust coalescence in a staggered rod bundle arrangement similar to that of the VHTR as well as locations of where graphite dust in the flow might act as wear particles and erode structural components in the lower plenum.

Ongoing experimental studies similar to that of Amini and Hassan have been recently performed at the matched index of refraction [MIR] facility at Idaho National Laboratory using a narrower channel [McIlroy Jr. *et al.* 2008]. The narrowed flow section is useful in studies of flows along the reflector wall of the lower plenum but eliminated flow features that are present away from the wall by the introduction of significant wall effects. The experimental data set of Amini and Hassan [2009] provides flow data for a wider range within the bundle as shown in Figure 1.

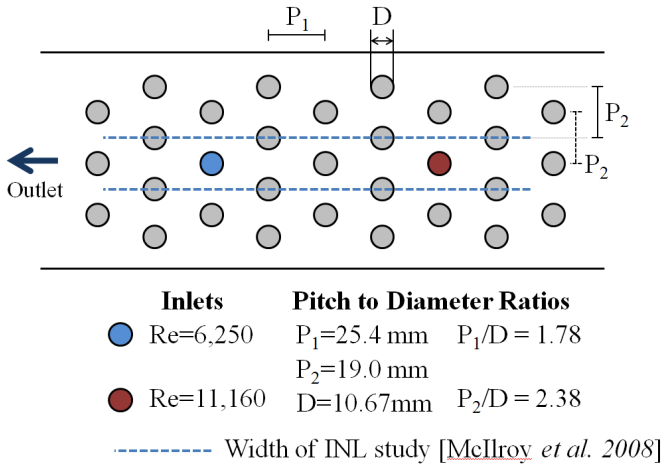

Figure 1. **Illustration of differences in experimental channel widths between Amini and Hassan's study and McIlroy Jr. *et al*'s**

Experimental flow visualization studies by Shu et al [2005] investigated the effect of nozzle shape on flow in water jets in the Reynolds number range of 5,000-10,000. In the case of the axis-symmetric round nozzle, the presence of strong Kelvin-Helmholtz instabilities in the range of 1-5 diameters was observed using the planar laser induced fluorescence (PLIF) technique as shown in Figure 2.

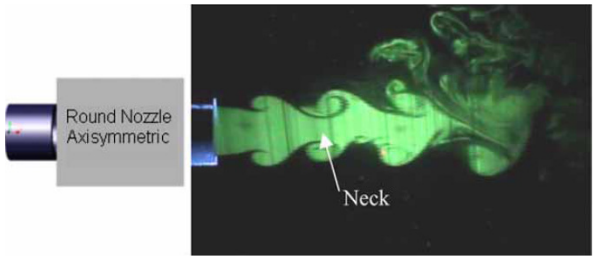

Figure 2. **Flow visualization of F. Shu *et al.*[2005] in which necking occurs in round jet of Re=5,000**

Numerous studies of vortex shedding following cylinders have been performed. Fey *et al.* [1998] developed a new Strouhal(St)-Reynolds number relationship based on experimental data for circular cylinders in uniform flows within the same Reynolds number range of interest as the present study. Other studies in the same Reynolds number range but of two in-line cylinders have been performed. Xu and Zhou [2004] found little to no detectable vortex shedding between the two cylinders for a distance of L/d<2; however, there was a rapid reduction in St behind the downstream cylinder as the gap increased from 1<L/d<2. Angrilli *et al.* [1982] investigated the influence of close proximity walls on the Strouhal number. Their investigation concluded that the wall increases the

Strouhal number slightly as it gets closer to the cylinder, thus increasing shedding frequency.

Vortex shedding frequency calculations using the equation for the Sr number should be approached with caution in the case of this study because of the non-uniformity of the flow field. The Strouhal-Reynolds number relationship developed by Roshko [1954] between Reynolds numbers of 300 and 10,000 gave a Strouhal number within 4% of the best fit of experimental data for uniform flow over a cylinder. While this error might be low for a linear approximation, the presence of a regime changes within this region should be noted. Like Roshko, Bloor [1963] observed irregularities in the 200<Re<400 range as well, but suggested that in this range turbulence was introduced by three dimensional effects. Above Re=400, transition takes place before the separation layer curls up. The regularities in the signals taken downstream of the cylinder were found to only occur when transition occurred well within the separated region. Bloor determined that regularities in the signal occurred for all Reynolds numbers above 1,300. The averaged Reynolds number was 4,641 in the lower plane region of the present study which put the flow regime past the cylinder above Bloor's criteria and near transition between the subcritical flow regime and the presence of Kelvin-Helmholtz instabilities in the shear layer [Fey *et al.* 1998]. As will be shown in the results of the present study, transition between high and lower fluctuation regimes appear to take place as the flow fluctuates in time.

NOMENCLATURE

GCI,	Grid convergence index
h,	Grid size
p,	Apparent order of convergence
r,	Grid size ratio
φ,	Extrapolated result
e,	Relative error

METHODOLOGY

In order to perform the desired CFD simulations, the fluid domain must first be discretized into small pieces over which the governing equations may be applied to obtain the results for a given mesh and numerical model. An important part of the discretization process is to ensure that numerical diffusion due to the size of the grid is kept to a minimum. In a subsequent section, the grid sensitivity study is discussed in detail.

DISCRETIZATION

The objective of any simulation is to obtain high fidelity results; however, many times the results are a product of artifacts of numerical diffusion as opposed to flow physics. A necessary measure to avoid such diffusion as much as possible is to perform a mesh sensitivity study to determine the cell size below which numerical artifacts don't present themselves on the scales of interest to the flow. Difficulties arise in such efforts with the advent of the unstructured mesh. In this work, unstructured polyhedral cells were used in the discretization process. In an effort to make the meshes more comparable to one another and limit error sources, a volume modifier was employed in the meshing process that forced the polyhedral cells into a semi-structured pattern within the volume. This helped homogenize the mesh throughout the domain of interest with the exception of very close to wall features that the mesh must adapt around. The prism layer for all of the meshes was maintained the same as to avoid introducing affects from other sources than the core polyhedral mesh.

The cell sizes within the bundle region of interest had cell sizes of 0.65mm, 0.75mm, 0.9mm, 1.2mm, 2mm, and 3mm. The parameters which were investigated for mesh convergence were velocity magnitudes taken along the axis of the jets from the jet entrance to the lower impingement plane. Figure 3 illustrates the mesh sizes of the different meshes taken along the mid-plane of the channel bisecting both inlet jets.

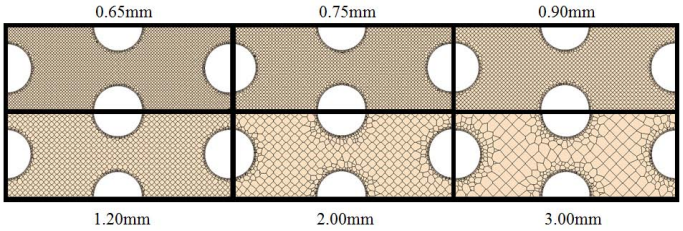

Grid Number	Cell Size (d_c) in mm	Number of Cells (N)	Cell-rod diameter ratio (d_c/D)
0	0.65mm	13,207,130	0.061
1	0.75mm	10,176,501	0.070
2	0.90mm	7,662,692	0.084
3	1.20mm	5,603,819	0.112
4	2.00mm	4,439,612	0.187
5	3.00mm	4,237,281	0.281

Figure 3. **Semi-structured polyhedral mesh metrics down to 0.65mm cell base diameter for sensitivity study**

Discretization error was quantified using the procedures outlined in the quality control statement of Celik et al. [2008] as well as Roache[1998] which outline accepted techniques by which the Richardson extrapolation(RE) method may be applied reliably. Local and average orders of accuracy, extrapolated results, percent errors, and grid convergence indexes were all calculated in accordance with these accepted

practices in an effort to ensure that high fidelity results had indeed been obtained.

All six generated meshes were investigated using the realizable k-ε turbulence model with an all-y+ wall function applied to a two cell prism layer that remained constant between the different grids. The steps by which RE was performed are as follows [Celik et al. 2008]:

Step 1

For grid sizes h1<h2<h3, where r21=h2/h1 and r32=h3/h2 are near or greater than 1.3, the local apparent order, p, of the simulation is calculated with the following expressions:

$$p = \frac{1}{\ln r_{21}} \left| \ln \left| \frac{\varepsilon_{32}}{\varepsilon_{21}} \right| + q(p) \right| \quad (1a)$$

$$q(p) = \ln \frac{(r_{21}^{p} - s)}{(r_{32}^{p} - s)} \quad (1b)$$

$$s = \sin\left(\frac{\varepsilon_{32}}{\varepsilon_{21}}\right) \quad (1c)$$

Where

$$\varepsilon_{21} = \varphi_2 - \varphi_1 \quad (2a)$$

$$\varepsilon_{32} = \varphi_3 - \varphi_2 \quad (2b)$$

Equation (1a-c) was solved using an iterative procedure with an initial guess of φ_1 where φ_n represents the result of the associated grid n.

Step 2

The extrapolated values φ_{ext}^{21} and φ_{ext}^{32} were calculated using the following equations:

$$\varphi_{ext}^{21} = \frac{(r_{21}^{p}\varphi_1 - \varphi_2)}{(r_{21}^{p} - 1)} \quad (3a)$$

$$\varphi_{ext}^{32} = \frac{(r_{32}^{p}\varphi_2 - \varphi_3)}{(r_{32}^{p} - 1)} \quad (3b)$$

Step 3

The relative errors e_a^{21} and e_{ext}^{21} were calculated with the expressions below:

$$e_a^{21} = \left| \frac{\varphi_1 - \varphi_2}{\varphi_1} \right| \quad (4a)$$

$$e_{ext}^{21} = \left| \frac{\varphi_{ext}^{21} - \varphi_1}{\varphi_{ext}^{21}} \right| \quad (4b)$$

Step 4

Calculate the grid convergence index for a fine mesh refinement with:

$$GCI_{fine}^{21} = F_s \frac{e_a^{21}}{r_{21}^{p_{ave}} - 1} \quad (5)$$

In eqn 5, the F_s coefficient serves as a 'buffer coefficient' for the extrapolated error approximation GCI. In the case of rough grids, a conservative value of 3 may be applied to this factor, and in the more refined grid cases, as in the case of this study, a value of 1.25 may be used[Roache 1998]. The idea behind this coefficient reducing to a value of 1 for a more refined grid is that as grid cell size gets smaller, the error due to numerical diffusion reduces to the point that any error present between the extrapolated solution and the calculated solution is the absolute error and is no longer an artifact of grid dependency, thus GCI = e in such a case.

The first investigated parameter in the sensitivity study was the velocity magnitude in the axial direction to the inlet jets at both locations (z=775mm and z=673.4) within the channel. For all cases, identical line probes sampled 30 points from the bottom of the channel to points within the inlet jet (y=0mm to y=78.2mm). Grid convergence indices were calculated based on three grids at a time. Grid combinations following the recommendation of having grid size ratios larger than 1.3 [Celik et al. 2008] were used; however, combinations were also used that intentionally violated this practice to investigate the scale of the error in the Richardson extrapolation. This grid sensitivity study was performed using two different Dirichlet boundary conditions, thus giving two separate sets of results using identical grids. Ensuring grid dependence for both cases further insures that the fidelity of the end result has not been compromised due to numerical diffusion, but instead any discrepancies between validation data and numerical results will be a direct result of the numerical model or models used.

GRID SENSITIVITY STUDY

The sensitivity results presented in this section pertain to axial flow velocity magnitude results taken in the axial direction of each jet plume for the case of Re_{jet1}=11,160 and Re_{jet2}=6,250. The percent errors shown in figure 4 are for the most refined grid from the extrapolated result using the method outlined in the previous section. The higher percent errors near y=0mm are expected as the impinging jet has a high velocity gradient at these locations and very subtle changes in velocity produce large percent errors here. For the present study, the results are taken as generally converged, but with the errors kept in mind.

In the case of the lower Reynolds number percent error, the reason for the dip to zero has to do with an oscillatory convergence of the results. Within the parameter investigated, the results of the line probe crossed each other which lead to an extrapolated result at this crossed point equal to the same value, hence, the error at this point presents itself as zero. The results of the sensitivity study found the minimum global orders of convergence amongst the parameters investigated to be 1.99 while most exceeded 3rd order. The results presented were said to be grid converged to second order accuracy.

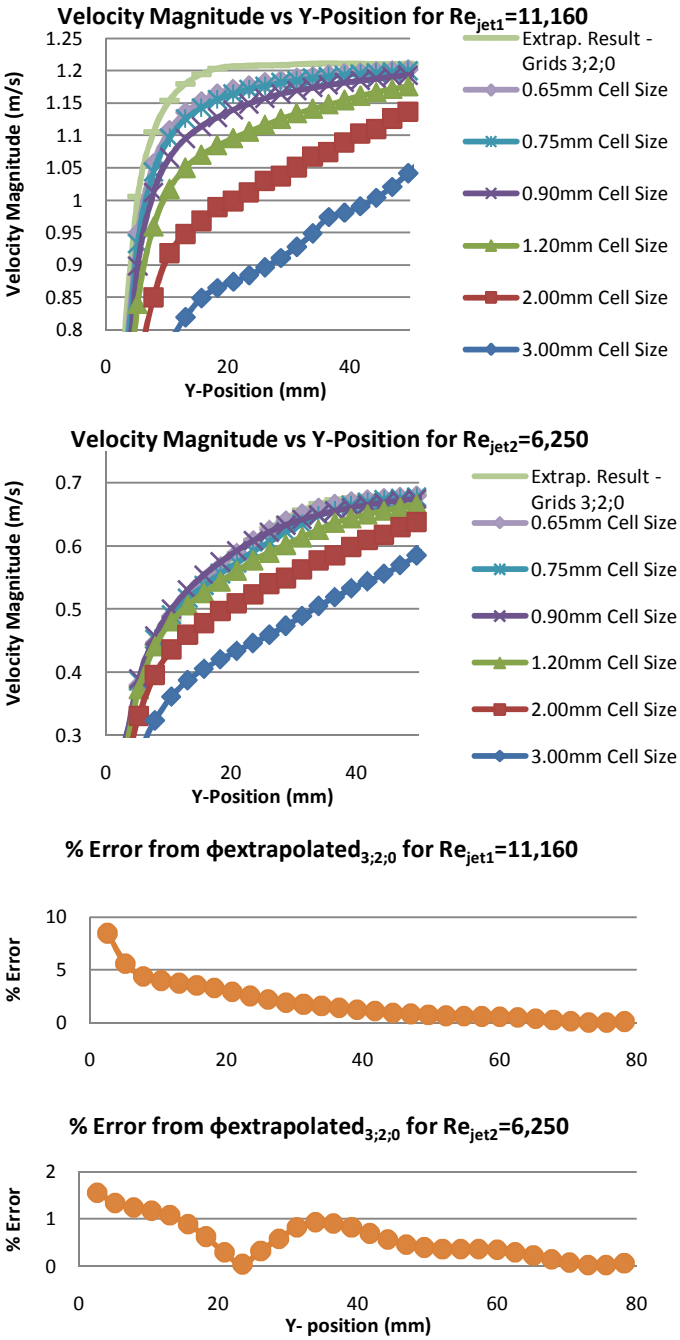

Figure 4. **Extrapolated results and from grids 3, 2, and 0 for Re$_{jet1}$=11,160 and Re$_{jet2}$=6,250 and the associated % errors for the smallest grid**

MODEL SPECIFICATIONS

The standard and realizable k-ε two equation models were used for the steady state simulations. A two layer all-y+ model utilizing the Wolfstein shear driven model [10] was applied to resolve all boundaries. The purpose of the steady state simulations was to perform a grid dependency study as well as identify potential regions of interest for result extraction in the unsteady simulation. The unsteady simulation was performed using a large eddy simulation (LES) solver which resolves the large scales by solving the Navier-Stokes formulation directly while solving for scales below the grid size using the wall adaptive local eddy-viscosity (WALE) subgrid scale model (SGS) [11]. It should be noted that a similar coefficient to that present in the Smagorinsky SGS model is used which has local influence on the flow; however, the level of influence of the coefficient is reduced with the WALE SGS model. For the present study, a coefficient C_w of 0.544 was used. The use of an implicit time stepping was chosen because the time scales of the flow phenomena are on the same scale as the convection and diffusion processes. The implicit solver enabled a relaxation of the Courant Friedrich Levi (CFL) condition to obtain satisfactory results (CFL<5).

The advantage to the use of an implicit solver is a drastic reduction in the computational time necessary to run the simulation until fully developed conditions have been reached in the flow. This is due to the ability to choose a time step nearly 10 times larger than that with an explicit solver. The selection of the time step for the LES simulation in this study was chosen from the CFL condition for the given length scales. The maximum velocity (~1.3m/s) in the flow domain occurs at the high Reynolds number jet entrance into the domain. The cell size is approximately 0.65mm and applying the CFL condition of 1, the time step chosen is 0.0005s.

Upon running the simulation, the maximum CFL number in the entire flow domain was a value of 2.08 and values in the range over 1 were only present in the core of the jet plume and not in the viscous superlayer where the jet entrains the semi-quiescent domain.

ANALYSIS METHODS

Advanced frequency analysis methods have been developed and employed heavily in recent years for the purpose of visualizing a decomposed frequency such that the frequencies present, intensities, and duration of specific frequencies throughout the length of the signal may all be obtained from a single plot. The idea behind wavelets takes root back to Joseph Fourier and his developed method now referred to as the Fourier transform [Fourier 1822] whereby sine and cosine waves could be superimposed to represent another function entirely.

The wavelet transform method of signal decomposition is a proven method that offers a very powerful method of signal analysis. In the case of the present study, convoluted signals are decomposed for analysis through this method.

The wavelet transform is a method by which a single defined wavelet basis function $\psi(t)$ is expanded in its range and domain as well as translated such that an entire series of functions or 'atoms' that are used to characterize the signal $s(t)$. The atoms are defined by the function $\psi_{a,b}(t)$ [Misiti *et al* 2007]:

$$\psi_{a,b}(\mathrm{t}) = \frac{1}{\sqrt{a}}\psi\left(\frac{t-b}{a}\right) \qquad (18)$$

Where coefficient b translates the wavelet basis function $\psi(\mathrm{t})$, and a adjusts the scale. The continuous wavelet transform of signal $s(t)$ is defined by the function C_f.

$$C_f(a,b) = \int_{\mathbb{R}} s(t)\overline{\psi_{a,b}(\mathrm{t})}\,dt \qquad (19)$$

The coefficients $C_f(a,b)$ give an indication of the level of correlation between the adjusted wavelet function and the signal for given values of a and b over the entire time domain. By plotting the coefficients over the entire domain with respect to time and scale, with color intensity indicating coefficient values, a logical depiction of the decomposed signal in the time domain may be viewed in a single plot.

NUMERICAL RESULTS

Jet Spreading Rate and the Viscous Superlayer

Steady state results, while not entirely representative of a flow dominated heavily by unsteady flow phenomena, are still useful in identifying regions of potential interest to be investigated in unsteady results, as well as good points of comparison with time averaged experimental data. The experimental data of Amini and Hassan [2009] is presented as an averaged velocity field obtained using dynamic 2D PIV. Comparison between simulation results using various numerical models and the experimental data was performed using line probes taken in the axial direction within each jet, and then plotted on the same axis for each jet. In addition to steady state models, averaging of the LES results was also performed over roughly 1400 time steps for a total simulation time of 0.7 seconds.

Jet dispersion is one parameter for comparison amongst the different models. An arbitrarily threshold value for the jet 'edge' was set to be 15% of the peak jet velocity obtained by the probe nearest to the inlet. This threshold value was kept constant for the remaining probes and was chosen due to it giving the best compromise between spreading and velocity field variation on the fringe of the jet. The following figures show jet widths at varying heights between the inlet and 1.1cm from the bottom plane of the channel.

	Low Jet	**High Jet**
Experimental Data	4.35°	2.60°
Standard k-epsilon	6.59°	3.46°
Realizable k-epsilon	5.95°	3.46°
LES	2.31°	2.15°

Figure 5. **Spreading angles of the two jets using different models**

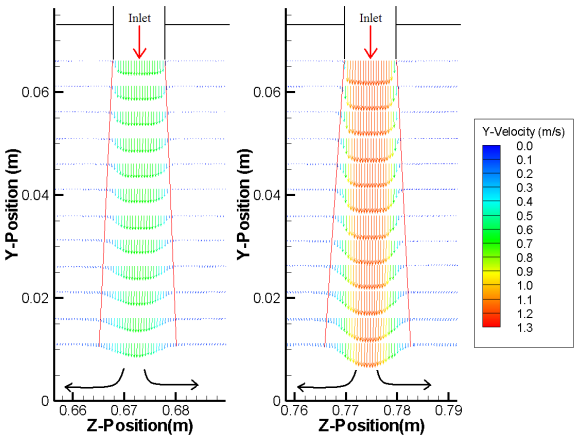

Figure 6. **Figure displaying velocity profiles along line probes of the averaged LES results for the two jets Re=6,250(left) and Re=11,160(right).**

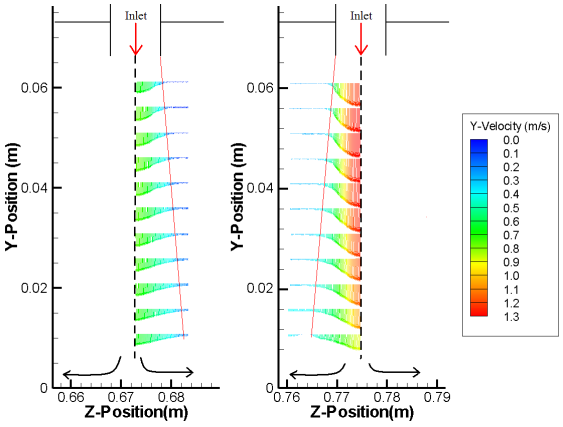

Figure 7. **Figure displaying velocity profiles along line probes of the averaged experimental data [Amini 2009] for the two jets Re=6,250(left) and Re=11,160(right).**

The velocity profiles at the jet nozzle outlets in both the experimental data and numerical results. The experimental data shows outlet conditions partway between a top-hat velocity profile and a Gaussian profile, whereas the numerical results have a well defined top-hat profile. The different profiles can have profound differences on the turbulent shear layer of the jet wake as demonstrated by New *et al* [2006]. It was shown that a top-hat velocity profile resulted in a dramatic reduction in the dimensionless length x/D to the formation of coherent vorticies in the shear layer around the jet plume. The results of the parabolic entrance profile are less coherent vortex structures and the increased disintegration of flow structures into small scale eddies.

Compiling the spreading jet diameters for all the models compared, as well as the experimental data [Amini and Hassan 2009] shown in figure 6, it is seen that in the case of the high velocity jet, the two variations of the k-epsilon model give

nearly identical spreading rates, while the averaged result of the LES simulation has far less diffusion. The experimental data falls between both the steady state models as well as the averaged LES results. The spreading angle of the jets may be estimated by taking the half angle of the linear extrapolations plotted in figure 6.

Recirculation Zones and the Horseshoe Vortex

A key phenomenon present within the lower plenum is the formation of recirculation zones. Within the lower plenum these may present the problem of hot spot formation along the support rods due to insufficient mixing. Recirculation zones present in the steady state results where the jet plumes impact the columns in the vertical mid-plane indicate the presence of horseshoe vorticies. Smaller secondary counter rotating vorticies are also present at the separation sites of the larger vorticies. In the experimental results [Amini and Hassan 2009], two dimensional PIV data was obtained in this vertical midplane. The time averaged data shows the two dominant recirculation zones; however, without three dimensional measurements the structure of the vorticies cannot be confirmed to indeed be horseshoe vorticies.

The importance of these horseshoe vorticies is threefold. The first is the formation of hotspots in these locations, the second is the possible scouring of the graphite support rods and lower plenum surrounding the base of the support rod, and the third is the buildup of graphite dust in the shadow zone following the rod. The nearly constant presence of high intensity horseshoe vorticies around the base of the cylinders would be points of high abrasion for a material prone to dust formation such as graphite. Muzzammil and Gangadhariah [2003] experimentally investigated the presence of the horseshoe vortex formed around the base of a pier column in a crossflow and the key role that is played by this vortex in the scour of the surrounding base. The insulation layer at the bottom of the lower plenum of the VHTR is composed of one meter of nuclear graphite and 200mm of carbon-carbon composite [MacDonald 2003]. Given sufficient wear particles present in the gas flow in addition to the low lubrication properties of graphite under low humidity and high temperature conditions, abrasion should be investigated further. If abrasive wear occurs at the location of a constant vortex, the presence of twin horseshoe vorticies on opposing sides due to multiple inlets might pose an added threat to the column integrity if sufficient material is lost. The presence of such abrasion in the actual reactor is still undetermined and the likelihood that it actually occurs in the lower plenum is still relatively unknown.

In the unsteady LES results, entrainment features are more readily identified than in the steady state results due to the averaging of the solutions. High jet entrainment of the surrounding semi-quiescent fluid is indicated by the streamline tendency towards the jets. Jet entrainment is highly dependent on interaction between the surrounding fluid and the jet at the viscous superlayer.

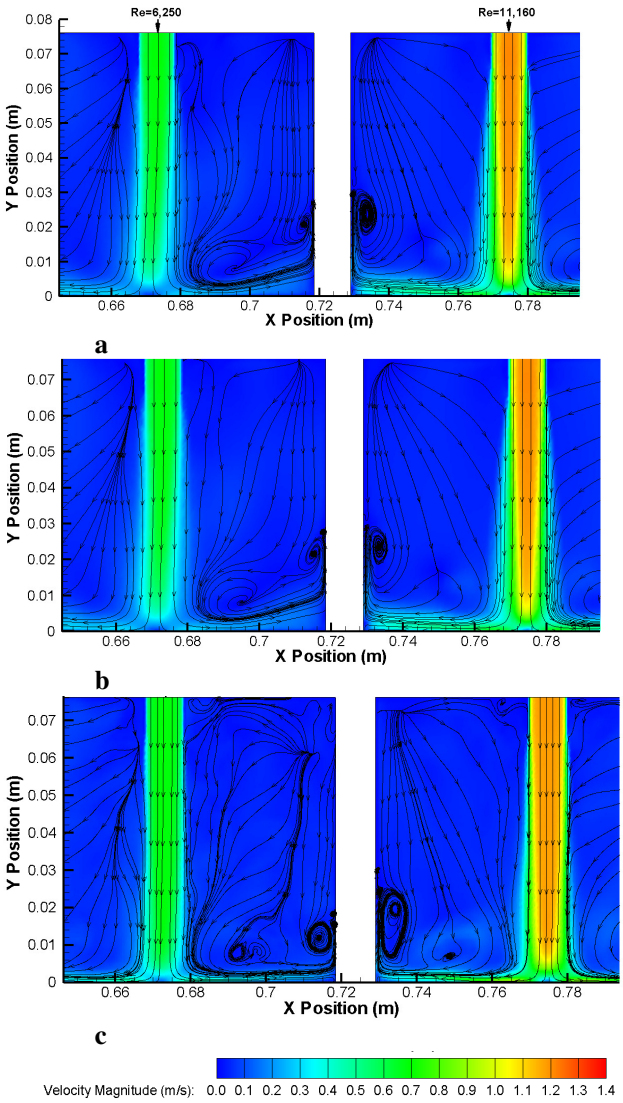

Figure 8. **Steady state results in the vertical mid-plane for the *a)*standard k-ε model, *b)* realizable k-ε model, and *c)* averaged results from the LES model**

The necking of the jet and formation of Kelvin-Helmholtz instabilities has been observed in experimental works for round jets in the same range of Reynolds numbers as investigated in the present work [F. Shu *et al.* 2005]. In the case of a jet that has a top-hat profile as opposed to a Gaussian profile, a reduced distance (x/D) to the onset of vortex rings has been documented [New *et al* 2006] and it is highly likely that the strong presence of these structures in the numerical results but not the experimental is likely due to slightly different entrance profiles causing different entrainment structures. The iso-surface plot in figure 10 as well as the velocity and vorticity fields in figure 11 shows the formation of tight vortex rings and high velocity in the jet at these necked locations due to the conservation laws.

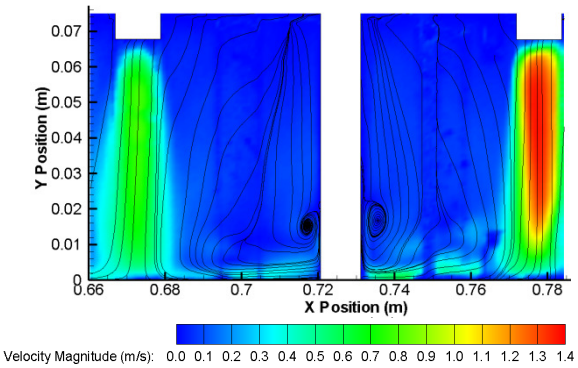

Figure 9. **Steady state results in the vertical mid-plane for the experimental data [Amini and Hassan 2009]**

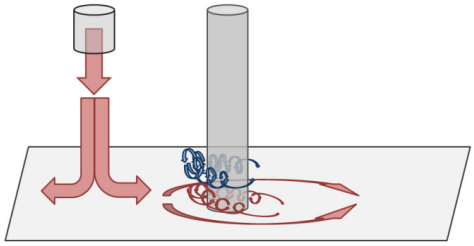

Figure 10. **Single and twin horseshoe vortices around a column**

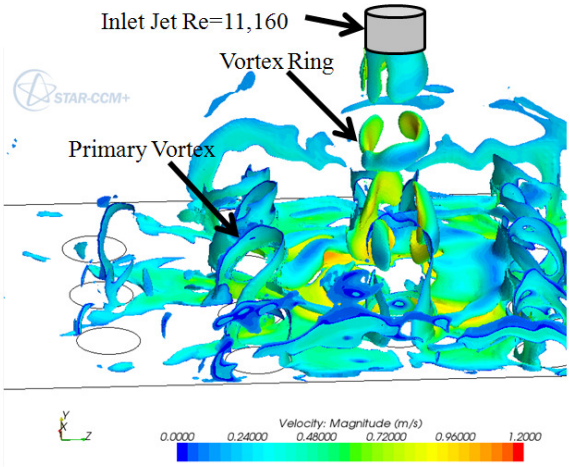

Figure 11. **Vorticity iso-surfaces with velocity magnitude scalar coloration of instantaneous LES results**

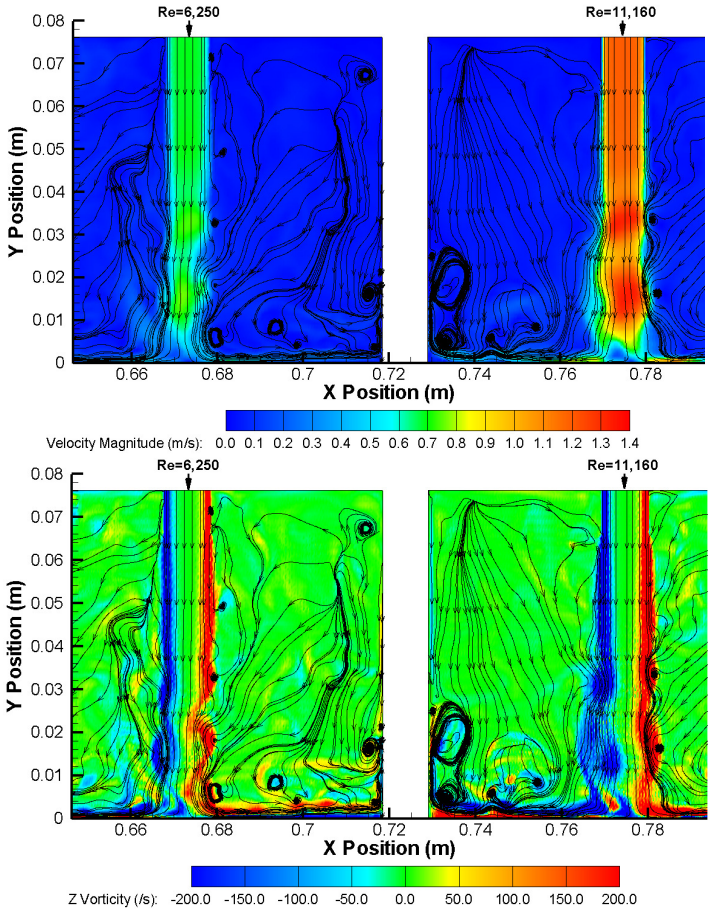

Figure 12. **Instantaneous velocities and out of plane Z vorticity components illustrating vortex structures in the viscous superlayer**

In the horizontal plane 2mm from the plane of impingement, shadow zones presented themselves in the results. Shadow zones are features observed in the wake of horseshoe vorticies just following the cylinder and before the onset of the turbulent instabilities. This phenomenon has been described by Greenly and Iverson [1985] as the reason for dust buildup just behind obstructions in windy conditions.

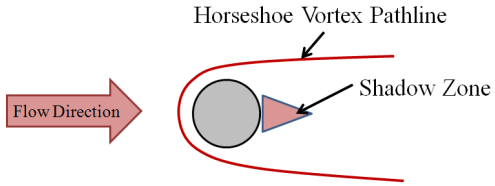

Figure 13. **Dead zone in the wake just following a cylindrical obstruction**

In the wake just following flow past the cylinders out of the mid-plane, shadow zones are observed for most locations, although the size and shape vary largely based on the location relative to the two impinging jets.

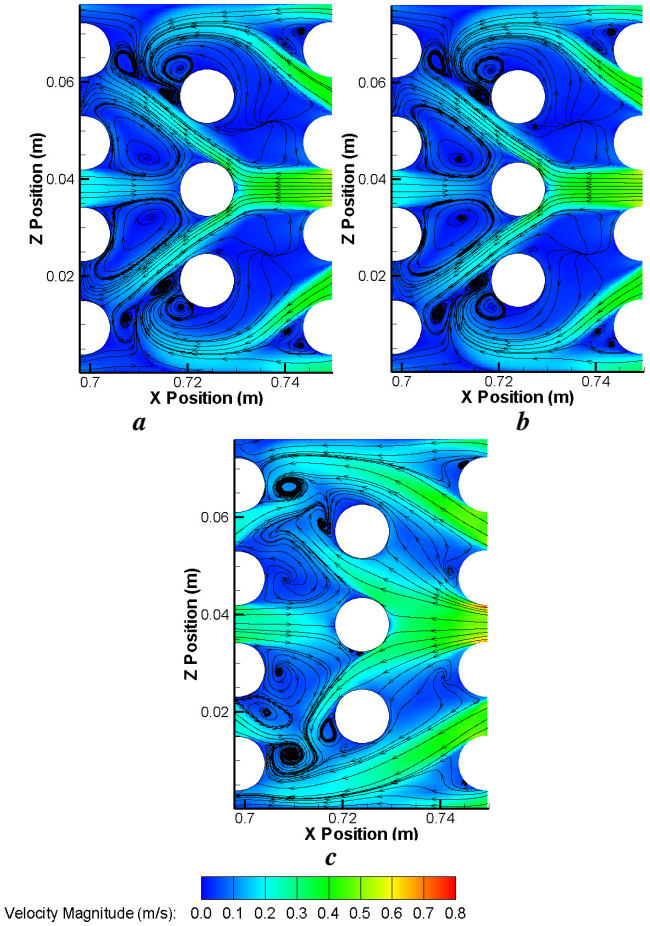

Figure 14. **Steady state results in the horizontal plane 2mm from the bottom plane for the *a)*standard k-ε model, the *b)* realizable k-ε model, and the *c)* averaged results from the LES model**

These results are in agreement with those seen by Johnson *et al* [2006] in which the presence of standing wakes downstream of the cylinders were seen. Their unsteady simulations and experimental data both confirm these shadow zones; however, at the time of the publication it was unsure as to the accuracy of both the numerical results and experimental data.

Wavelet Transform Frequency Analysis

A difficulty in the analysis of unsteady CFD simulations is the amount of information present in the results. To focus the scope of this work, instantaneous signals extracted from the results in the vertical mid-plane bisecting the two inlets are investigated.

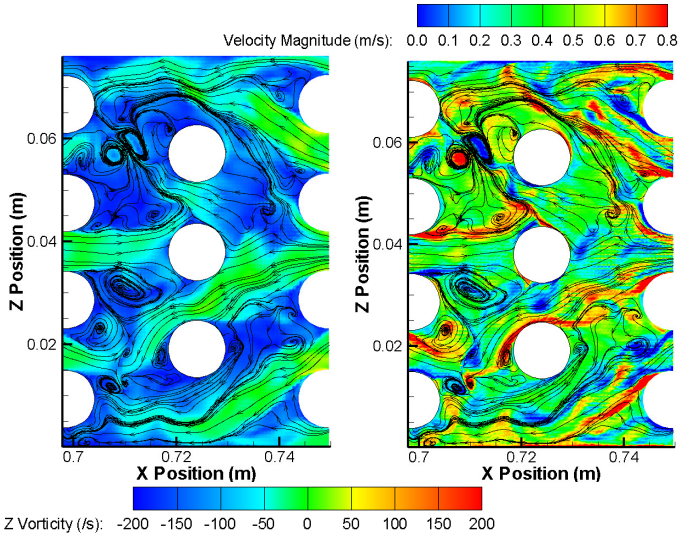

Figure 15. **Instantaneous LES results of velocity(left) and out of plane vorticity(right) scalars.**

Signals were extracted from the results at the locations shown in figure 16. The continuous wavelet transform was used to break down the signal and determine the dominant frequencies by applying high and low pass filters that employ a 'mother wavelet'. Depending on which mother wavelet is used, different information and features of the signal may be extracted. The wavelet decomposition plot of the signal seen in figure 17 may be interpreted as an instantaneous decomposition of a signal. At any given time, *t*, the contour in the y direction will give the frequencies present at that time and the relative intensities of each by the non-dimensional contour level.

The Morlet mother wavelet is useful in identifying sharp gradients in the signal. This characteristic ability gives it particularly good frequency resolution as opposed to some of the other mother wavelets. The continuous wavelet decomposition of the velocity signals in figure 17 of point 10 illustrates the dominant frequency induced by the periodic entrainment of surrounding fluid in a location two diameters from the jet inlet. The contour levels indicate intensity of the frequency present going from blue on the low end to red on the high intensity end. The dominant frequency present occurs around at 45Hz. The decomposition of a signal obtained 6.5 diameters from the inlet jet is shown in figure 17 as point 2. The dominant frequency remains the same as before; however, the intensity has amplified as vortex formation caused an increase in core velocity inside the jet.

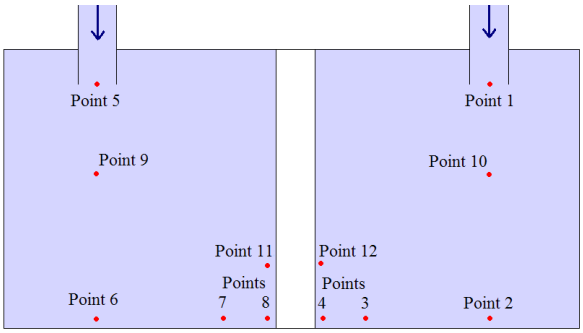

Figure 16. **Extraction points along the vertical mid-plane for wavelet analysis**

As the impinged jet spreads, turbulence induced by the presence of out of plane rods as well as turbulent spots along the lower plane of the channel alter the characteristic frequencies in the flow. The decompositions of points 3 and 4 further along the lower impingement plane show newly introduced turbulent frequencies due to these other sources. Comparison of the four decompositions at high temporal frequencies shows the highly periodic nature of the flow seen at the inlet and additional decompositions throughout the domain should be performed so that frequencies may be traced throughout the domain and the points of origin understood.

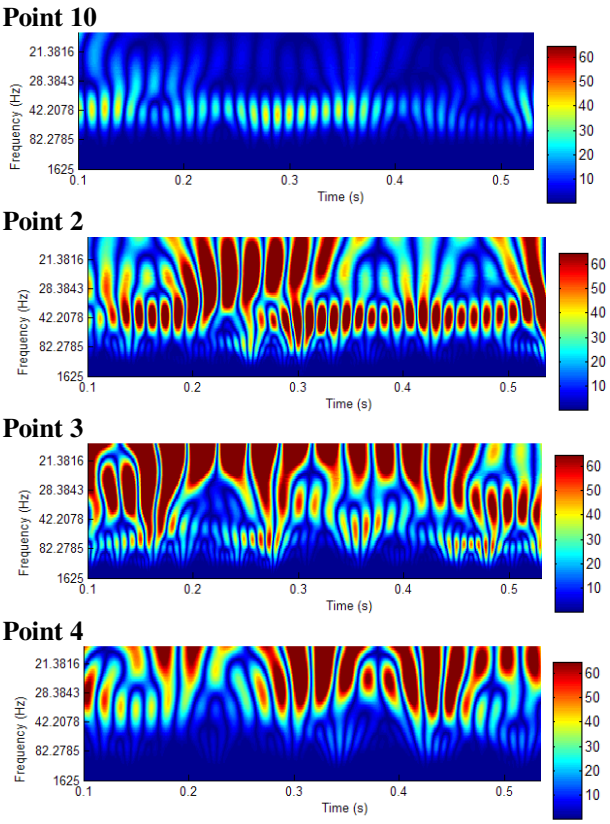

Figure 17. **Wavelet decompositions of four point signals taken in the vertical mid-plane of the**

While the presence of strong periodic perturbations at the inlet jet plume location seem to have mostly been lost in the signal at point 3, point 4 shows the onset of a new dominant frequency around the 25Hz band.

CONCLUSION

Analyses of steady and unsteady simulations have been performed in the present study and several features have been successfully identified from the numerical results and confirmed against experimental work [Amini and Hassan 2009]. The effect of the jet velocity profile appears to have affected how the flow structure entrains the surrounding fluid; however, further investigation of the effect of the profile in rod bundles is still needed. If the profile is crucial in the generation of strong Kelvin-Helmholtz instabilities in a distance y/D that falls within the lower plenum region, additional work needs to be done on the actual inlet conditions within VHTR as this will greatly affect the phenomena present in the support column structure.

Despite the presence of strong frequency generation in the jet entrainment, the presence of fairly constant horseshoe vorticies around the support columns still occurs. These vorticies need to be investigated further in terms of possible abrasion of the nuclear graphite in the lower plenum support structure.

ACKNOWLEDGMENTS

The lead author would like to acknowledge Dr.Yassin Hassan's support for the present study as well as the insight from other colleagues at Texas A&M University, namely Noushin Amini and Carlos Estrada.

REFERENCES

Angrilli, F., Bergamaschi, S., Cossalter, V., 1982. Investigation of Wall Induced Modifications to Vortex Shedding From a Circular Cylinder. J. of Fluids Eng., Vol. 104, pp.518-522.

Amini N., Hassan Y. A., 2009. PIV Measurements of Jet Flows Impinging Into a Channel Containing a Rod Bundle Using Dynamic PIV. Int. J. of Heat and Mass Transfer, Vol. 52, Issues 23-24, pp. 5479-5495.

CD-Adapco Group, 2008. Star-CCM+ Methodology and User Guide. Version 3.02.006.

Celik, I.B., Ghia, U., Roache, P.J., Freitas, C.J., Coleman, H., Raad, P.E., 2008. Procedure for Estimation and Reporting of Uncertainty Due to Discretization in CFD Applications. J. of Fluids Eng., vol 130, issue 7.

Fey, U., König, M., Eckelmann, H., 1998. A new Strouhal-Reynolds Number Relationship for the Circular Cylinder in the Range 47<Re<2e10. Physics of Fluids. Vol. 10, issue 7, pp.1547-1549.

Fourier, J., 1822. Théorie Analytique de la Chaleur, Paris.

Greeley, R., Iversen, J.D., 1985. Wind as a Geological Process on Earth, Mars, Venus, and Titan, Cambridge Univ. Press, New York. pp. 333.

Johnson, R.W., Guillen, D.P., Gallaway, T., 2006. Investigations of the Application of CFD to Flow Expected in the Lower Plenum of the Prismatic VHTR. Idaho National Laboratory. INL/EXT-06-11756, pp.53-54.

Jones, W.P. and Lander, B.E. 1972. The Prediction of Laminarization with a Two-Equation Model of Turbulence. Int. J. Heat and Mass Transfer, vol. 15, pp. 301-314.

Launder, B.E. and Sharma, B.I., 1974. Application of the Energy Dissipation Model of Turbulence to the Calculation of Flow Near a Spinning Disc. Letter in Heat and Mass Transfer, vol. 1, no. 2, pp 131-138.

MacDonald, P.E., 2003. NGNP Preliminary Point Design – Results of the Initial Neutronics and Thermal-Hydraulics Assessments. Idaho National Engineering and Environmental Laboratory. INEEL/EXT-03-00870, pp.17.

McIlroy Jr., H.M., McEligot, D.M., Pink, R.J., 2008. Measurement of Turbulent Flow Phenomena for the Lower Plenum of a Prismatic Gas-Cooled Reactor. Nucl. Eng. Des., doi:10.1016/j.nucengdes.2008.07.020

Misity, M., Misity, Y., Oppenheim, G., Poggi, J.-M., 2007. Wavelets and their Applications. ISTE Ltd., pp.2-6.

Muzzammil, M., Gangadhariah, T., 2003 The Mean Characteristics of Horseshoe Vortex at a Cylindrical Pier. Journal of Hydraulic Research. pp. 285-299.

New, T.H., T.T. Lim, and S.C. Luo, 2006. Effects of Jet Velocity Profiles on a Round Jet in Cross-flow." Experiments in Fluids. Vol.40, pp. 859-875.

Roache, P.J., 1998. Verification and Validation in Computational Science and Engineering. Hermosa Publishers.

Rodriguez, S.B., El-Genk, M.S., 2008. Using Helicoids to Eliminate 'Hot Streaking' in the VHTR Lower Plenum. International Congress on Advances in Nuclear Power Plants,.

Shih, T.-H., Liou, W.W., Shabbir, A., Yang, Z. and Zhu, J., 1995. A New k-Eddy Viscosity Model for High Reynolds Number Turbulent Flows -- Model Development and Validation. Computers and Fluids, Vol. 24, No. 3, pp. 227-238.

Shu, F., Plesniak, M.W., Sojka, P.E., 2005. Intermediate-origin Noxxles to Control Jet Structure and Evolution. Journal of Turbulence, Vol 6, No. 26.

Xu, G., Zhou, Y., 2004. Strouhal Numbers in the Wake of Two Inline Cylinders. Expt. In Fluids. pp.248-256.